A CLASS OF BUBBLE ENRICHED QUADRATIC FINITE VOLUME ELEMENT SCHEMES ON TRIANGULAR MESHES

YANHUI ZHOU

Abstract. In this work, we propose and analyze a class of bubble enriched quadratic finite volume element schemes for anisotropic diffusion problems on triangular meshes. The trial function space is defined as quadratic finite element space by adding a space which consists of element-wise bubble functions, and the test function space is the piecewise constant space. For the class of schemes, under the coercivity result, we proved that $|u - u_h|_1 = \mathcal{O}(h^2)$ and $\|u - u_h\|_0 = \mathcal{O}(h^3)$, where u is the exact solution and u_h is the bubble enriched quadratic finite volume element solution. The theoretical findings are validated by some numerical examples.

Key words. Bubble enriched quadratic finite volume element schemes, anisotropic diffusion problems, triangular meshes, H^1 and L^2 error estimates.

1. Introduction

Due to the local conservation law and other advantages, the finite volume method (FVM) is one of the most important numerical methods for solving partial differential equations, see e.g. [2, 21, 30, 31, 34]. The finite volume element (FVE) method (FVEM) is a special type of FVM, and attracted many researchers attention (e.g. [22, 25, 43]).

The coercivity result is a basis for the error estimate of FVEM. For the linear FVEM over triangular meshes, its element stiffness matrix can be regarded as a small perturbation of linear finite element method for variable coefficient, the coercivity result then follows (c.f. [1, 4, 16, 17, 38]). However, the coercivity analysis for the quadratic scheme is not easy. For instance, assume that the maximum angle of each triangular element is not greater than $90°$, and the ratio of the lengths of the two sides of the maximum angle belong to $[\sqrt{2/3}, \sqrt{3/2}]$, then Tian and Chen [33] presented a coercivity result for the first proposed quadratic scheme in 1991. In 1996, Liebau [24] proposed another quadratic scheme, and required that the geometry of the triangulation triangles is not too extreme. In 2009, Xu and Zou [38] introduced a general framework to construct quadratic schemes, and improved some coercivity results for the schemes presented in [15, 24, 33] . In 2012, Chen, Wu and Xu [11] presented a general framework for construction and analysis of higher-order FVMs, under their framework, the minimum angle conditions of the schemes in [15, 24, 33] are same as the results in [38]. In 2017, Zou [48] presented an unconditionally stable quadratic scheme. In 2020, Zhou and Wu [45, 46] improved some coercivity results, e.g., the minimum angle condition for the quadratic scheme presented in [36] is improved to $1.42°$. Therefore, most existing coercivity results of quadratic schemes required a certain minimum angle condition. Some studies about other types of hybrid FVMs and Hermite FVMs were presented in [6, 11, 12] and so on, and some coercivity results on quadrilateral meshes can be found in [7, 18, 22, 23, 29, 32, 41, 44, 47] and the references cited therein. Once the coercivity result is proved, the error estimate in H^1 norm is then routine.

However, the L^2 error estimate is much more difficult compared with H^1 error analysis. For example, for the linear FVEM over triangular meshes, by assuming that the exact solution $u \in W^{3,p}(\Omega)$, $p > 1$, in 1994 Chen [9] given a proof of optimal convergence order of L^2 error estimate. In 1998, Huang and Xi [19] present a counterexample to show that the optimal second order accuracy of L^2 error norm cannot be achieved by only assuming that $(u, f) \in H^2 \times L^2$, where f is the right hand side function. In 2002, Chen, Li and Zhou [10] discussed the optimal L^2 error estimate of linear FVEM, they proved that the L^2 error can be bounded by $h^2|\ln h|^{1/2}\|f\|_{1,1}$ and $h^2\|f\|_{1,p}$, $p > 1$. In 2002, Ewing, Lin and Lin [16] proved that the L^2 error can be bounded by $h^2\|u\|_2 + h^{1+\beta}\|f\|_\beta$ for $0 < \beta \le 1$. Recently, by introducing two orthogonal conditions on triangular meshes, in 2016 Wang and Li [36] constructed k-order FVE schemes such that the L^2 error can be bounded by $h^{k+1}\|u\|_{k+2}$. Some L^2 error estimates on quadrilateral meshes can be found in [26, 27, 28, 29, 42] for an incomplete references.

Therefore, one can observe that the theoretical analysis of quadratic FVEM on triangular meshes has not been developed satisfactorily. On the one hand, under a certain minimum angle condition $1.42°$ for the isotropic diffusion problems, the quadratic scheme in [36] can ensure the optimal L^2 error order. On the other hand, the unconditionally stable quadratic scheme presented in [48] does not guarantee the optimal convergence order in L^2 norm, at least it seems so numerically. Namely, in the exiting literature the quadratic scheme in [36] is the unique scheme such that the optimal L^2 error estimate holds, while the scheme in [48] is the unique unconditionally stable scheme. At this stage, in order to satisfy the wide applications of quadratic FVEM (e.g. [8, 14, 20, 35, 37, 39, 40]), it requires us make efforts to construct an unconditionally stable quadratic FVE scheme with the optimal L^2 error estimate. However, by the existing analysis techniques, it is difficult to find a quadratic FVE scheme such that the local coercivity result (independent of the minimum angle of underlying mesh) and optimal L^2 error estimate holds simultaneously.

Unlike the existing quadratic FVE schemes, in this work we propose a class of bubble enriched quadratic FVE schemes such that the H^1 (resp. L^2) error order is 2 (resp. 3). Precisely, by adding a space which consists of element-wise bubble functions to the standard quadratic finite element space, we obtain a class of FVE schemes with three scheme parameters α, β_1 and β_2, where $\alpha \in (0, 1/2)$ on the element boundary and $0 < \beta_1 < 2/3 < \beta_2 < 1$ in the interior of element. For some special schemes, by element analysis, we numerically show that the local coercivity result is valid on a class of isosceles triangles. When $\alpha = (3 - \sqrt{3})/6$, β_1 and β_2 satisfy (15) (or equivalently (18)), under the coercivity result, we proved that $|u - u_h|_1 = \mathcal{O}(h^2)$. Moreover, by the Aubin-Nitsche technique and assuming that $u \in H^3(\Omega)$, $f \in H^2(\Omega)$, we proved that $\|u - u_h\|_0 = \mathcal{O}(h^3)$ for these schemes. Finally, the theoretical results are verified by several numerical examples.

For the class of schemes presented in this paper, we may find a scheme such that the local coercivity result holds in future. Moreover, the existence of a class of FVE schemes can be used to attack many complicated problems. For example, we may search this class for a scheme which satisfied some additional properties, such as the positivity-preserving.

The rest part of this paper is organized as follows. In Section 2 we present a class of bubble enriched quadratic FVE schemes on triangular meshes. The coercivity result and H^1 error estimates of these schemes are discussed in Section 3. In Section 4, we proved that the L^2 error order is 3 of these schemes when the scheme

parameters $\alpha = (3 - \sqrt{3})/6$, β_1 and β_2 satisfy (15). In Section 5 some numerical examples are presented to validate the theoretical findings, and in Section 6 we make conclusive remarks. Throughout the paper, we will follow the usual notations "$\lesssim$", "$\gtrsim$" and "$\sim$" to avoid the repetition.

2. A class of bubble enriched quadratic FVE schemes

We consider the following elliptic equation

$$-\nabla \cdot (\Lambda \nabla u) = f \quad \text{in } \Omega, \tag{1}$$

$$u = 0 \quad \text{on } \partial\Omega, \tag{2}$$

where $\Omega \subset \mathbb{R}^2$ is a convex bounded polygonal domain, u is the function to be found, $f \in L^2(\Omega)$ and the coefficient $\Lambda = (\lambda_{ij}(x,y))$ is a 2×2 symmetric and uniformly positive definite matrix, i.e., there exist two positive constants $\underline{\lambda}$ and $\overline{\lambda}$ such that for all $(x,y) \in \Omega$

$$\underline{\lambda}\|\boldsymbol{v}\|^2 \le \boldsymbol{v}^T \Lambda \boldsymbol{v} \le \overline{\lambda}\|\boldsymbol{v}\|^2, \quad \forall \boldsymbol{v} \in \mathbb{R}^2, \tag{3}$$

where $\|\cdot\|$ is the Euclidean norm.

Suppose that the domain Ω is divided into a *primal mesh* $\mathcal{T}_h$ consisting of a finite number of non-overlapped triangles, where h is the largest diameter of all triangles. For each triangular element $K \in \mathcal{T}_h$, we denote by $\mathcal{N}_K$ the set of all three vertices, three edge midpoints and the barycenter of K; $\mathcal{E}_K$ the set of three edges of K. Let

$$\mathcal{N}_h = \bigcup_{K \in \mathcal{T}_h} \mathcal{N}_K, \quad \mathcal{N}_h^\circ = \mathcal{N}_h \backslash \partial\Omega, \quad \mathcal{E}_h = \bigcup_{K \in \mathcal{T}_h} \mathcal{E}_K.$$

The mesh $\mathcal{T}_h$ is called *shape regular* if for each triangle $K \in \mathcal{T}_h$, there exists a positive constant C_{sr} independent of h and K, such that $h_K/\rho_K \le C_{sr}$, where h_K is the largest diameter of K and ρ_K is the maximum diameter of circles contained in K. In this work, we require the discontinuity of diffusion coefficient Λ does not appear in the interior of each K.

Next, we present the dual mesh of Ω. To this end, we introduce some notations. For each $K = \triangle P_1 P_2 P_3 \in \mathcal{T}_h$, see Figure 1, let Q be the barycenter of K and M_i $(i = 1, 2, 3)$ be the midpoint of the line segment $P_i P_{i+1}$, here and hereafter i denotes, without special mention, a periodic index with period 3. For any $\alpha \in (0, 1/2)$, $P_{i,i+1}^\alpha$ and $P_{i+1,i}^\alpha$ are the two points on the line segment $P_i P_{i+1}$, subjected to

$$\frac{|P_i P_{i,i+1}^\alpha|}{|P_i P_{i+1}|} = \frac{|P_{i+1,i}^\alpha P_{i+1}|}{|P_i P_{i+1}|} = \alpha. \tag{4}$$

For any given $0 < \beta_1 < 2/3 < \beta_2 < 1$, let the points $P_{i,i+1}^{\beta_1}$ and $P_{i,i+1}^{\beta_2}$ on the line segment $P_i M_{i+1}$, satisfying

$$\frac{|P_i P_{i,i+1}^{\beta_1}|}{|P_i M_{i+1}|} = \beta_1, \quad \frac{|P_i P_{i,i+1}^{\beta_2}|}{|P_i M_{i+1}|} = \beta_2. \tag{5}$$

Using these notations, we reach a partition of K, consisting of three quadrilaterals and four pentagons, see Figure 1. For each node $P \in \mathcal{N}_h$, the dual cell associated with P is a polygonal domain surrounding P and denoted as $\mathcal{V}_P$. If $P = P_i$ is a vertex of K, then the contribution of K to $\mathcal{V}_P$ is the quadrilateral $\mathcal{V}_{K,P_i} := P_i P_{i,i+1}^\alpha P_{i,i+1}^{\beta_1} P_{i,i+2}^\alpha$, see Figure 2(a). If $P = M_i$ is an edge midpoint of K, then the contribution of K to $\mathcal{V}_P$ is the pentagon $\mathcal{V}_{K,M_i} := P_{i,i+1}^\alpha P_{i+1,i}^\alpha P_{i+1,i+2}^{\beta_1} P_{i+2,i}^{\beta_2} P_{i,i+1}^{\beta_1}$, see Figure 2(b). If $P = Q$ is a barycenter of K, then the contribution of K to $\mathcal{V}_P$ is the pentagon $\mathcal{V}_{K,Q} := P_{12}^{\beta_1} P_{31}^{\beta_2} P_{23}^{\beta_1} P_{12}^{\beta_2} P_{31}^{\beta_1} P_{23}^{\beta_2}$, see Figure 2(c). Then, the whole
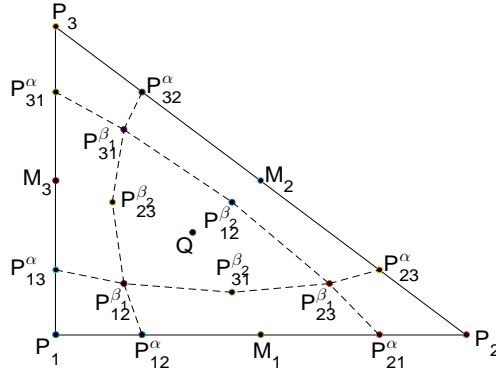
FIGURE 1. Partition of the triangular element K.

(a) vertex   (b) midpoint   (c) barycenter
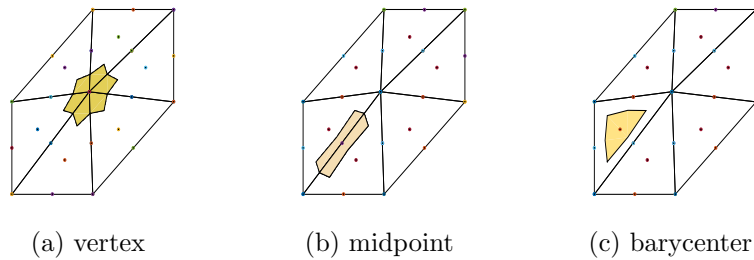
FIGURE 2. Dual cells associated with an interior vertex (left), an edge midpoint (middle) and a barycenter (right).

dual cell surrounding the point P is given by

$$\mathcal{V}_P = \bigcup_{\overline{K} \ni P} \mathcal{V}_{K,P}.$$

The *dual mesh* $\mathcal{T}_h'$ consists of all dual cells, that is

$$\mathcal{T}_h' = \{\mathcal{V}_P : P \in \mathcal{N}_h\},$$

see Figure 3 for an example of $\mathcal{T}_h'$.

Based on the meshes $\mathcal{T}_h$ and $\mathcal{T}_h'$, we define the corresponding trial function space and test function space, respectively. Firstly, with respect to the primal mesh $\mathcal{T}_h$, we denote the standard Lagrange finite element space as

(6) $$U_h^k = \{u_h \in C(\overline{\Omega}) : u_h|_K \in \mathbb{P}_k, \ \forall K \in \mathcal{T}_h; \ u_h|_{\partial\Omega} = 0\},$$

where $\mathbb{P}_k$ is the set of all polynomials of degree equal to or less than k. For any $\beta_2 \in (2/3, 1)$, we define the space of bubble functions

$$B_h = \{b_h \in C(\overline{\Omega}) : b_h|_K \in \mathrm{Span}\{(\beta_2 - 2/3)\lambda_1\lambda_2\lambda_3\}, \ \forall K \in \mathcal{T}_h\},$$

where $\lambda_i \ (i = 1, 2, 3)$ are the three linear nodal basis functions of K, in other words,

$$\lambda_i(P_j) = \delta_{ij} := \left\{ \begin{array}{ll} 1, & i = j, \\ 0, & i \neq j, \end{array} \right. \ i, j = 1, 2, 3.$$

The *trial function space* U_h is given by

(7) $$U_h = U_h^2 \oplus B_h.$$
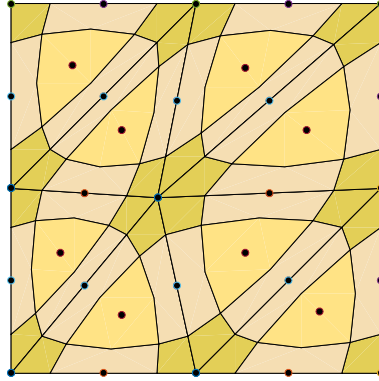
FIGURE 3. The primary mesh $\mathcal{T}_h$ and its associated dual mesh $\mathcal{T}_h'$.

Then, the $u_h \in U_h$ can be represented as

$$u_h|_K = \sum_{i=1}^{3} u_h(P_i)\phi_{P_i} + \sum_{i=1}^{3} u_h(M_i)\phi_{M_i}$$

$$(8) \qquad + 3\lambda_1\lambda_2\lambda_3 \left(9u_h(Q) + \sum_{i=1}^{3} u_h(P_i) - 4\sum_{i=1}^{3} u_h(M_i) \right),$$

where

$$(9) \qquad\qquad \phi_{P_i} = \lambda_i(2\lambda_i - 1), \quad \phi_{M_i} = 4\lambda_i\lambda_{i+1}.$$

Since the bubble function $\lambda_1\lambda_2\lambda_3$ is vanish on the boundary of K, we have u_h is continuous on Ω and thus $U_h \in H_0^1(\Omega)$.

Secondly, the *test function space* V_h contains all the piecewise constant functions with respect to $\mathcal{T}_h'$ defined as

$$(10) \qquad\qquad V_h = \text{Span}\{\psi_P : P \in \mathcal{N}_h^\circ\},$$

where ψ_P is the characteristic function on $\mathcal{V}_P$. Then from (7) and (10), we have

$$(11) \qquad\qquad \dim U_h = \dim V_h = \#\mathcal{N}_h^\circ,$$

where $\dim S$ and $\#S$ are the dimension and cardinality of the set S. We remark that the points $P_{12}^{\beta_2}$, $P_{23}^{\beta_2}$ and $P_{31}^{\beta_2}$ coincide with the barycenter Q when $\beta_2 = 2/3$, see Figure 1. The corresponding dual partition of K can be seen in Figure 4 and the trial function space U_h degenerate into the standard quadratic finite element space U_h^2, i.e., the $u_h \in U_h$ can be represented as

$$u_h|_K = \sum_{i=1}^{3} u_h(P_i)\phi_{P_i} + \sum_{i=1}^{3} u_h(M_i)\phi_{M_i}.$$

In this case, the equality (11) also holds by letting the set $\mathcal{N}_h^\circ$ exclude all the barycenters.

The bubble enriched quadratic finite volume element solution of Eqs. (1) and (2) is a function $u_h \in U_h$ which satisfies the following local conservation law

$$-\int_{\partial\mathcal{V}_P} (\Lambda\nabla u_h) \cdot \boldsymbol{n}\, \mathrm{d}s = \int_{\mathcal{V}_P} f\, \mathrm{d}x\mathrm{d}y$$
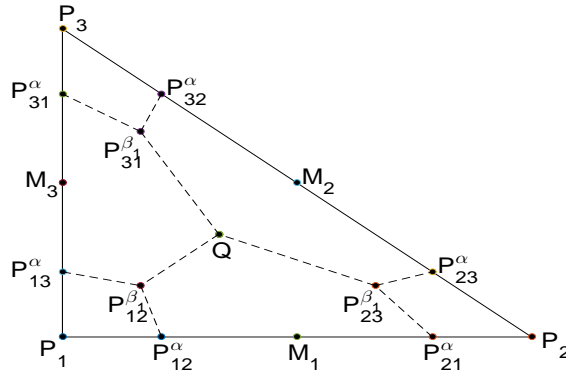
FIGURE 4. Partition of the triangular element K, where $\beta_2 = 2/3$.

on each dual cell $\mathcal{V}_P$, $P \in \mathcal{N}_h^\circ$, where $\boldsymbol{n}$ is the unit outward normal on the boundary $\partial \mathcal{V}_P$. For any $v_h \in V_h$, we have $v_h = \sum_{P \in \mathcal{N}_h^\circ} v_P \psi_P$, where the coefficients $v_P = v_h(P)$. Then the above bubble enriched quadratic finite volume element schemes for solving (1) and (2) can be rewritten as: Find $u_h \in U_h$ such that

$$(12) \qquad a_h(u_h, v_h) = (f, v_h), \quad \forall\, v_h \in V_h,$$

where the finite volume element bilinear form

$$(13) \qquad a_h(u, v_h) = - \sum_{P \in \mathcal{N}_h^\circ} v_P \int_{\partial \mathcal{V}_P} (\Lambda \nabla u) \cdot \boldsymbol{n}\, \mathrm{d}s, \quad u \in H_0^1(\Omega),\ v_h \in V_h$$

and (f, v_h) denotes the standard L^2 inner product of f and v_h.

From the construction of the dual mesh, one can see that it depends on three parameters $\alpha \in (0, 1/2)$, $\beta_1 \in (0, 2/3)$ and $\beta_2 \in (2/3, 1)$. Hence, (12) actually leads to a class of quadratic finite volume element schemes. In this paper, we consider a special class of schemes, i.e.,

$$(14) \qquad \alpha = \frac{3 - \sqrt{3}}{6},$$

the β_1 and β_2 satisfy
(15)
$$4 + 9\left(1 - \frac{1}{\sqrt{3}}\right)\left(-4 - \frac{2}{\sqrt{3}} + 3\beta_1\right)\beta_1 + 2\left(-1 - \frac{3}{2}\beta_1 + 3\beta_2\right)(2 - 3\beta_1)(3\beta_2 - 2) = 0.$$

In the following discussion, we shall to prove that if α satisfies (14), β_1 and β_2 satisfy (15), then the finite volume element solution u_h converges to exact solution u with convergence order 3 under L^2 error norm.

To this end, we first explore the Eq. (15). Discard the unreasonable solutions, there are infinitely many pairs $0 < \beta_1 < 2/3 \le \beta_2 < 1$ which satisfy (15). In fact, (15) is equivalent to

$$(16) \qquad c_2 \beta_2^2 + c_1 \beta_2 + c_0 = 0,$$

where
(17)
$$c_2 = 9, \quad c_1 = -\frac{9}{2}(2 + \beta_1), \quad c_0 = 2 + 3\beta_1 + \frac{4 + 9\left(1 - \frac{1}{\sqrt{3}}\right)\left(-4 - \frac{2}{\sqrt{3}} + 3\beta_1\right)\beta_1}{2(2 - 3\beta_1)}.$$
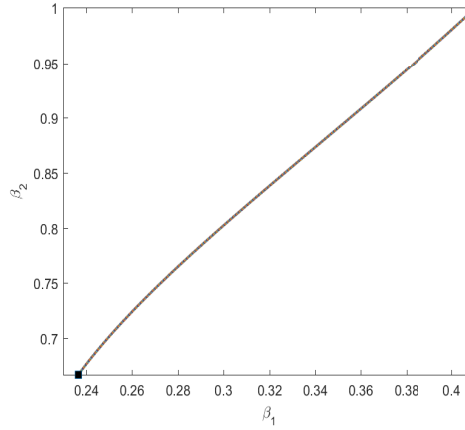
FIGURE 5. The relationship of β_1 and β_2 which satisfy (15) (or equivalently (18)).

Suppose that

$$\beta_2^{\pm} = \frac{-c_1 \pm \sqrt{c_1^2 - 4c_2 c_0}}{2c_2}$$

are the two roots of (16). Then, we have $\beta_2^- \le \beta_2^+$ and

$$2\beta_2^- \le \beta_2^- + \beta_2^+ = -\frac{c_1}{c_2} = 1 + \frac{\beta_1}{2} < \frac{4}{3},$$

which implies that $\beta_2^- < 2/3$. Consequently, the reasonable solution of (16) is

$$(18) \qquad \beta_2 = \beta_2^+ = \frac{-c_1 + \sqrt{c_1^2 - 4c_2 c_0}}{2c_2},$$

where c_2, c_1 and c_0 are defined in (17), and

$$\beta_1 \in \left[\frac{6 + \sqrt{3} - \sqrt{21 + 6\sqrt{3}}}{9}, \ \frac{29 + 4\sqrt{3} - \sqrt{265 + 76\sqrt{3}}}{39} \right).$$

The relationship of (18) is graphically depicted in Figure 5. Moreover, from (18), we can derive some special pairs of (β_1, β_2) by a direct calculation, for example

$$
\begin{aligned}
&\beta_1 = \frac{6 + \sqrt{3} - \sqrt{21 + 6\sqrt{3}}}{9} \approx 0.2366, \ \beta_2 = \frac{2}{3}; \\
(19) \qquad &\beta_1 = \frac{1}{4}, \ \beta_2 = \frac{135 + \sqrt{5265 - 2400\sqrt{3}}}{240} \approx 0.7012; \\
&\beta_1 = \frac{1}{3}, \ \beta_2 = \frac{7 + \sqrt{25 - 8\sqrt{3}}}{12} \approx 0.8615.
\end{aligned}
$$

We mention that for the first pair of parameters (β_1, β_2) in (19), see also the '■' in Figure 5, since $\beta_2 = 2/3$, then it is identical to the quadratic scheme in [36]. The rest part of this paper is devoted to the H^1 and L^2 error estimates of these schemes.

3. Coercivity and H^1 error estimates

In this section, for the α satisfies (14), $\beta_1 \in (0, 2/3)$ and $\beta_2 \in (2/3, 1)$ satisfy (15), we numerically discuss the coercivity result by element analysis. Based on the coercivity result, we prove that the finite volume element solution converges to exact solution with convergence order 2 under H^1 error norm.

3.1. Preliminaries. For a given $\omega \neq 0$, suppose that the mapping Π maps a $u_h \in U_h$ to $u_h^* := \Pi u_h \in V_h$, satisfying for each vertex P_i,

$$u_h^*(P_i) = u_h(P_i), \quad i = 1, 2, 3,$$

and for each midpoint M_i,

$$(20) \qquad u_h^*(M_i) = \frac{1-\omega}{2}\left(u_h(P_i) + u_h(P_{i+1})\right) + \omega u_h(M_i), \quad i = 1, 2, 3,$$

and for each barycenter Q,

$$u_h^*(Q) = u_h(Q).$$

We remark that if $\omega = 1$ (resp. $\omega = 2/\sqrt{3}$), then (20) reduces to the mapping in [22, 33] (resp. [45, 48]). Obviously, the mapping Π is a bijection.

To prove the global coercivity result

$$(21) \qquad a_h(u_h, u_h^*) \gtrsim |u_h|_1^2, \quad \forall\, u_h \in U_h,$$

it suffices to prove

$$(22) \qquad a_h^K(u_h, u_h^*) \gtrsim |u_h|_{1,K}^2, \quad \forall\, u_h \in U_h,\ \forall\, K \in \mathcal{T}_h,$$

where

$$a_h^K(u_h, u_h^*) = -\sum_{P \in \mathcal{N}_h} u_h^*(P) \int_{\partial \mathcal{V}_P \cap K} (\Lambda \nabla u_h) \cdot \boldsymbol{n}\, ds.$$

From (8), we have

$$u_h|_K = \sum_{i=1}^3 u_h(P_i)\varphi_{P_i} + \sum_{i=1}^3 u_h(M_i)\varphi_{M_i} + u_h(Q)\varphi_Q,$$

where

$$\varphi_{P_i} = \phi_{P_i} + 3\lambda_1\lambda_2\lambda_3, \quad \varphi_{M_i} = \phi_{M_i} - 12\lambda_1\lambda_2\lambda_3, \quad \varphi_Q = 27\lambda_1\lambda_2\lambda_3, \quad i = 1, 2, 3.$$

For any $\omega \neq 0$, by (9), it is trivial to verify

$$(23) \qquad \sum_{i=1}^3 \varphi_{P_i} + \sum_{i=1}^3 \varphi_{M_i} + \varphi_Q = \sum_{i=1}^3 \varphi_{P_i}^* + \sum_{i=1}^3 \varphi_{M_i}^* + \varphi_Q^* = 1.$$

For any $u_h \in U_h$, in each K, we define the vector

$$(24) \qquad \boldsymbol{u} = (u_h(P_1), \cdots, u_h(P_6), u_h(P_7))^T,$$

where $P_{i+3} := M_i$, $i = 1, 2, 3$ and $P_7 := Q$. Hence, there holds

$$(25) \qquad a_h^K(u_h, u_h^*) = a_h^K\left(\sum_{j=1}^7 u_h(P_j)\varphi_{P_j},\ \sum_{i=1}^7 u_h(P_i)\varphi_{P_i}^*\right) = \boldsymbol{u}^T \mathbb{A}_K \boldsymbol{u},$$

where $\mathbb{A}_K = (a_{ij})_{7\times 7}$ with

$$(26) \qquad a_{ij} = a_h^K(\varphi_{P_j}, \varphi_{P_i}^*).$$

Lemma 3.1. *Assume that $\mathcal{T}_h$ is shape regular, then for each $K \in \mathcal{T}_h$,*

$$(27) \qquad\qquad |u_h|_{1,K} \sim \|\mathbb{G}\boldsymbol{u}\|, \quad \forall\, u_h \in U_h,$$

where

$$(28) \qquad \mathbb{G} = \begin{pmatrix} 1 & 0 & 0 & 0 & -1 & 0 & 0 \\ 0 & 1 & 0 & 0 & 0 & -1 & 0 \\ 0 & 0 & 1 & -1 & 0 & 0 & 0 \\ 0 & 0 & 0 & 1 & -1 & 0 & 0 \\ 0 & 0 & 0 & 0 & 1 & -1 & 0 \\ 1 & 1 & 1 & -4 & -4 & -4 & 9 \end{pmatrix},$$

$\boldsymbol{u}$ is defined in (24).

Proof. Since $\mathcal{T}_h$ is shape regular, then by a scaling argument, we have

$$|u_h|_{1,K} \sim |u_h|_{1,\widehat{K}}, \quad \forall\, K \in \mathcal{T}_h,$$

where $\widehat{K}$ is the reference triangular element consists of three vertices $(0,0)$, $(1,0)$ and $(0,1)$. Note that $|u_h|_{1,\widehat{K}} = 0$ is equivalent to u_h being a constant function, which holds if and only if

$$u_h(P_1) = \cdots = u_h(P_6), \quad 9u_h(Q) + \sum_{i=1}^{3} u_h(P_i) - 4\sum_{i=1}^{3} u_h(M_i) = 0,$$

and if and only if

$$(29) \qquad\qquad u_h(P_1) = \cdots = u_h(P_6) = u_h(Q).$$

On the other hand, we also have $\|\mathbb{G}\boldsymbol{u}\| = 0$ if and only if (29) holds. That is, $|u_h|_{1,\widehat{K}}$ and $\|\mathbb{G}\boldsymbol{u}\|$ are all positive semi-definite quadratic forms of $u_h(P_i)$, $i = 1, \cdots, 7$, and have the same null-subspaces, thus the desired result (27) is proved. $\qquad\square$

Lemma 3.2. *Let*

$$(30) \qquad \mathbb{T} = \frac{1}{63} \begin{pmatrix} 55 & -8 & -8 & -21 & 21 & -1 \\ -8 & 55 & -8 & -21 & -42 & -1 \\ -8 & -8 & 55 & 42 & 21 & -1 \\ -8 & -8 & -8 & 42 & 21 & -1 \\ -8 & -8 & -8 & -21 & 21 & -1 \\ -8 & -8 & -8 & -21 & -42 & -1 \\ -15 & -15 & -15 & 0 & 0 & 6 \end{pmatrix}$$

and define

$$\mathbb{B}_K = \frac{1}{2}\mathbb{T}^T \left(\mathbb{A}_K + \mathbb{A}_K^T \right) \mathbb{T},$$

where $\mathbb{A}_K$ is given by (26). *Then we have*

$$(31) \qquad\qquad \mathbb{G}^T \mathbb{B}_K \mathbb{G} = \frac{1}{2} \left(\mathbb{A}_K + \mathbb{A}_K^T \right).$$

Proof. Firstly, we claim that

$$(32) \qquad\qquad \sum_{k=1}^{7} a_{ik} = \sum_{k=1}^{7} a_{kj} = 0, \quad i, j = 1, \cdots, 7.$$

Actually, it follows from (26) and (23) that

$$\sum_{k=1}^{7} a_{ik} = \sum_{k=1}^{7} a_h^K (\varphi_{P_k}, \varphi_{P_i}^*) = a_h^K \left(\sum_{k=1}^{7} \varphi_{P_k}, \ \varphi_{P_i}^* \right) = a_h^K (1, \varphi_{P_i}^*) = 0, \quad i = 1, \cdots, 7$$

and

$$\sum_{k=1}^{7} a_{kj} = a_h^K \left(\varphi_{P_j}, \ \sum_{k=1}^{7} \varphi_{P_k}^* \right) = a_h^K(\varphi_{P_j}, 1) = 0, \quad j = 1, \cdots, 7,$$

where we have used the fact that $\Lambda \nabla \varphi_{P_j}$ is continuous across the dual edges inside K.

Secondly, by (28) and (30), we find that

$$\text{(33)} \qquad\qquad\qquad\qquad \mathbb{T}\mathbb{G} = \mathbb{I} - \frac{1}{7}\mathbb{1},$$

where $\mathbb{I}$ is the identity matrix and $\mathbb{1}$ is a 7×7 matrix with all entries equal to 1.

Finally, we deduce from (33) and (32) that

$$\left(\mathbb{A}_K + \mathbb{A}_K^T \right) \mathbb{T}\mathbb{G} = \mathbb{A}_K + \mathbb{A}_K^T - \frac{1}{7}(\mathbb{A}_K + \mathbb{A}_K^T)\mathbb{1} = \mathbb{A}_K + \mathbb{A}_K^T,$$

which leads to (31). □

3.2. The coercivity result. In order to present the coercivity result, we introduce the following assumption.

(**A1**) For the α satisfies (14), $\beta_1 \in (0, 2/3)$ and $\beta_2 \in (2/3, 1)$ satisfy (15) (or equivalently (18)), $\mathbb{B}_K$ is a uniformly positive definite matrix.

Theorem 3.1. *Assume that $\mathcal{T}_h$ is shape regular, then under the assumption (**A1**), the coercivity result (21) holds.*

Proof. Under the assumption (**A1**), for any $K \in \mathcal{T}_h$, it follows from (25), (31) and (27) that, for any $u_h \in U_h$,

$$a_h^K(u_h, u_h^*) = \boldsymbol{u}^T \mathbb{A}_K \boldsymbol{u} = \frac{1}{2}\boldsymbol{u}^T \left(\mathbb{A}_K + \mathbb{A}_K^T \right) \boldsymbol{u} = (\mathbb{G}\boldsymbol{u})^T \mathbb{B}_K (\mathbb{G}\boldsymbol{u}) \gtrsim \|\mathbb{G}\boldsymbol{u}\|^2 \sim |u_h|_{1,K}^2,$$

which validates (22) and then (21). □

In the rest part of this subsection, for the scheme derived from (15), we numerically discuss the positive definiteness of $\mathbb{B}_K$ on isosceles triangular element. For simplicity, we assume that Λ is an identity matrix on K.

Firstly, we set

$$\omega_i = \omega_L + \frac{\omega_R - \omega_L}{N_\omega}(i - 1), \quad 1 \le i \le N_\omega + 1,$$

where $N_\omega = 200$, ω_L and ω_R are two parameters.

Secondly, for each ω_i, the mapping Π can be uniquely determined by (20), then we compute its corresponding minimum angle condition $\theta_{\min}^i$ on a class of isosceles triangular elements $K_j = \triangle P_1^j P_2 P_3$. Specifically, we assume the coordinates $P_1^j(1/2, h_j)$, $P_2(0,0)$ and $P_3(1,0)$, where $h_j = (\sqrt{3}j)/(2N_t)$, $j = 1, \cdots, N_t$ and $N_t = 200$. For the ω_i, its corresponding smallest angle and 6×6 symmetric matrix of K_j are denoted by $\arctan(2h_j)$ and $\mathbb{B}_{K_j}^i$ respectively. Then, we let

(34)

$$\theta_{\min}^i = \min_{1 \le j_0 \le N_t} \left\{ \arctan\left(2h_{j_0}\right) : \mathbb{B}_{K_j}^i \text{ is a positive definite matrix for all } j_0 \le j \le N_t \right\}.$$

The numerical results of two special schemes are presented in Figure 6, where the horizontal coordinate is the ω, while the vertical coordinate is its corresponding minimum angle condition computed by (34). In Figure 6(a), we choose $\omega_L = 0.3$ and $\omega_R = 2$. In Figure 6(b), we choose $\omega_L = 0.22$ and $\omega_R = 0.8$.
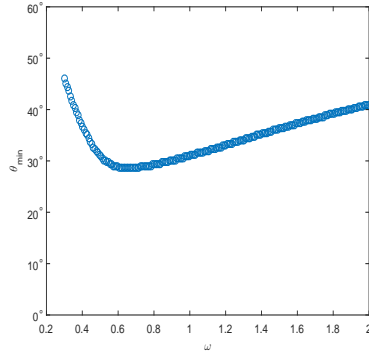
(a) $\beta_1 = 1/4$, $\beta_2 = (135 + \sqrt{5265 - 2400\sqrt{3}})/240$
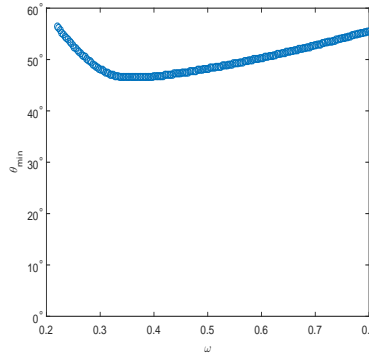
(b) $\beta_1 = 1/3$, $\beta_2 = (7 + \sqrt{25 - 8\sqrt{3}})/12$

FIGURE 6. The effect of ω to the minimum angle condition on isosceles triangle.

The numerical results of the schemes (15) are presented in Figure 7(a), where the horizontal coordinate is the β_1. In Figure 7(a), we choose $\omega_L = 0.2$ and $\omega_R = 2$, and $\theta_{\min}$ is computed by

$$\theta_{\min} = \min_{1 \le i \le N_\omega} \theta^i_{\min},$$

where $\theta^i_{\min}$ is defined by (34). Moreover, the numerical results of the schemes α satisfies (14), $\beta_1 \in (0, 2/3)$ and $\beta_2 \in (2/3, 1)$ are presented in Figure 7(b). From Figures 6 and 7, we can see that for the α satisfies (14), $\beta_1 \in (0, 2/3)$ and $\beta_2 \in (2/3, 1)$ satisfy (15), the assumption (**A1**) is valid under a certain minimum angle condition.

3.3. H^1 error estimates. By a routine work, we have the following H^1 error estimates.

Theorem 3.2. *Assume that $\mathcal{T}_h$ is shape regular and the exact solution $u \in H_0^1(\Omega) \cap H^3(\Omega)$. Then, under the assumption (**A1**), we have*

(35) $$|u - u_h|_1 \lesssim h^2 \|u\|_3.$$

Proof. It follows from the Green's formula that

$$a_h(u, v_h) = (f, v_h), \quad \forall v_h \in V_h,$$

(a) the schemes (15)   (b) the schemes $\beta_1 \in (0, 2/3)$, $\beta_2 \in (2/3, 1)$
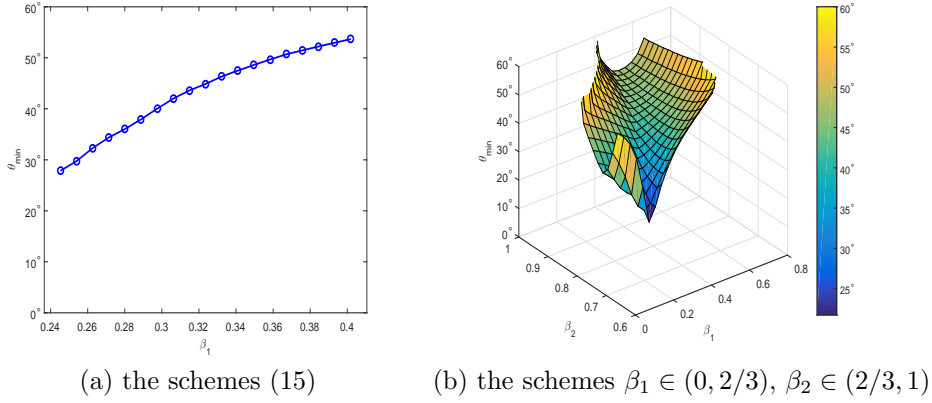
FIGURE 7. The minimum angle conditions of some special schemes on isosceles triangle.

which leads to

$$a_h(u - u_h, v_h) = 0, \quad \forall \, v_h \in V_h.$$

Therefore, by (21) and the continuity of $a_h(\cdot, \cdot)$ (c.f. [38]), we deduce that

$$|u_h - u_I|_1^2 \lesssim a_h \left(u_h - u_I, (u_h - u_I)^* \right) = a_h \left(u - u_I, (u_h - u_I)^* \right)$$

$$\lesssim \left(\sum_{K \in \mathcal{T}_h} \left(|u - u_I|_{1,K}^2 + h_K^2 |u - u_I|_{2,K}^2 \right) \right)^{\frac{1}{2}} |u_h - u_I|_1,$$

where $u_I \in U_h^2$ is the piecewise quadratic interpolation of u such that for each triangular element K

$$u_I(P_i) = u(P_i), \ u_I(M_i) = u(M_i), \quad i = 1, 2, 3.$$

Consequently, by the standard interpolation error estimate [3, 13], we find that

$$|u_h - u_I|_1 \lesssim h^2 \|u\|_3,$$

which yields to (35). □

4. L^2 error estimates

In this section, for a class of schemes α satisfies (14), $\beta_1 \in (0, 2/3)$ and $\beta_2 \in (2/3, 1)$ satisfy (15), we use the Aubin-Nitsche technique to obtain the L^2 error estimates.

4.1. Preliminaries.

Lemma 4.1. *If α satisfies* (14), *then for each edge $e \in \mathcal{E}_h$, we have*

$$(36) \qquad \int_e v(w - w^*) \, \mathrm{d}s = 0, \quad \forall \, v \in U_h^2, \ w \in U_h^1,$$

where U_h^1 and U_h^2 are defined by (6).

Proof. For each edge $e \in \mathcal{E}_h$, let P_1 and P_2 be the two endpoints, and M_1 be the midpoint, c.f. Figure 1. Note that on the edge e, each $v \in U_h^2$ and $w \in U_h^1$ can be represented as

$$v = v(P_1)\lambda_1 + v(P_2)\lambda_2 + \left(v(M_1) - \frac{v(P_1) + v(P_2)}{2} \right) 4\lambda_1 \lambda_2$$

and
$$w = w(P_1)\lambda_1 + w(P_2)\lambda_2$$
respectively. To prove (36), it suffices to validate (36) for $v = \lambda_1$ and $w = \lambda_1$, $v = \lambda_2$ and $w = \lambda_1$, $v = \lambda_1\lambda_2$ and $w = \lambda_1$.

Firstly, we consider the case $v = \lambda_1$ and $w = \lambda_1$. A direct calculation yields that
$$\int_e vw \, \mathrm{d}s = \int_e \lambda_1^2 \, \mathrm{d}s = \frac{1}{3}|e|.$$
On the other hand, the facts
$$w^* = 1, \quad \text{on edge } P_1 P_{12}^\alpha,$$
$$w^* = \frac{1}{2}, \quad \text{on edge } P_{12}^\alpha P_{21}^\alpha,$$
$$w^* = 0, \quad \text{on edge } P_{21}^\alpha P_2$$
yield that
$$\int_e vw^* \, \mathrm{d}s = \int_e \lambda_1 \lambda_1^* \, \mathrm{d}s = \int_{P_1 P_{12}^\alpha} \lambda_1 \, \mathrm{d}s + \frac{1}{2}\int_{P_{12}^\alpha P_{21}^\alpha} \lambda_1 \, \mathrm{d}s = \frac{1}{3}|e|.$$

Secondly, we consider the case $v = \lambda_2$ and $w = \lambda_1$. By a straightforward calculation, we deduce that
$$\int_e vw \, \mathrm{d}s = \int_e \lambda_1 \lambda_2 \, \mathrm{d}s = \frac{1}{6}|e|$$
and
$$\int_e vw^* \, \mathrm{d}s = \int_e \lambda_2 \lambda_1^* \, \mathrm{d}s = \int_{P_1 P_{12}^\alpha} \lambda_2 \, \mathrm{d}s + \frac{1}{2}\int_{P_{12}^\alpha P_{21}^\alpha} \lambda_2 \, \mathrm{d}s = \frac{1}{6}|e|.$$

Finally, we consider the case $v = \lambda_1\lambda_2$ and $w = \lambda_1$. Still by a direct calculation, we have
$$\int_e vw \, \mathrm{d}s = \int_e \lambda_1^2 \lambda_2 \, \mathrm{d}s = \frac{1}{12}|e|$$
and
$$\int_e vw^* \, \mathrm{d}s = \int_e (\lambda_1\lambda_2) \lambda_1^* \, \mathrm{d}s = \int_{P_1 P_{12}^\alpha} \lambda_1\lambda_2 \, \mathrm{d}s + \frac{1}{2}\int_{P_{12}^\alpha P_{21}^\alpha} \lambda_1\lambda_2 \, \mathrm{d}s = \frac{1}{12}|e|.$$

By the same arguments, (36) holds for $v = \lambda_2$ and $w = \lambda_2$, $v = \lambda_1$ and $w = \lambda_2$, $v = \lambda_1\lambda_2$ and $w = \lambda_2$. This completes the proof. □

Lemma 4.2. *For any α defined by (4), $\beta_1 \in (0, 2/3)$ and $\beta_2 \in (2/3, 1)$ defined by (5), we have*

$$(37) \qquad \int_K (w - w^*) \, \mathrm{d}x\mathrm{d}y = 0, \quad \forall w \in U_h^1, \ K \in \mathcal{T}_h.$$

Moreover, if α satisfies (14), $\beta_1 \in (0, 2/3)$ and $\beta_2 \in (2/3, 1)$ satisfy (15), then

$$(38) \qquad \int_K v(w - w^*) \, \mathrm{d}x\mathrm{d}y = 0, \quad \forall v \in U_h^1, \ w \in U_h^1, \ K \in \mathcal{T}_h.$$

Proof. Note that
$$U_h^1 = \mathrm{Span}\{\lambda_1, \lambda_2, \lambda_3\}$$
in K, to prove (37), it suffices to verify (37) for $w = \lambda_1$. A straightforward calculation yields that
$$\int_K w \, \mathrm{d}x\mathrm{d}y = \int_K \lambda_1 \, \mathrm{d}x\mathrm{d}y = \frac{1}{3}|K|.$$

By the definition of the mapping Π, we find that

$$w^* = 1, \text{ in polygon } \mathcal{V}_{K,P_1},$$

$$w^* = \frac{1}{2}, \text{ in polygons } \mathcal{V}_{K,M_1} \text{ and } \mathcal{V}_{K,M_3},$$

$$w^* = \frac{1}{3}, \text{ in polygon } \mathcal{V}_{K,Q},$$

$$w^* = 0, \text{ in polygons } \mathcal{V}_{K,P_2}, \ \mathcal{V}_{K,M_2} \text{ and } \mathcal{V}_{K,P_3}.$$

Suppose that the areas of $\triangle P_1 P_{12}^{\alpha} P_{12}^{\beta_1}$ and $\triangle P_{12}^{\beta_1} P_{31}^{\beta_2} Q$ are S_1 and S_2, respectively. Then

$$\int_K \lambda_1^* \, \mathrm{d}x\mathrm{d}y = \frac{1}{3}|K|,$$

where we have used the fact that

$$|\mathcal{V}_{K,M_1}| = |\mathcal{V}_{K,M_3}| = \frac{1}{3}|K| - 2S_1 - 2S_2.$$

That is, (37) holds for $w = \lambda_1$. Similarly, (37) is valid for $w = \lambda_2$ and λ_3.

We next prove (38). Firstly, for the special functions $v = \lambda_2$ and $w = \lambda_1$, we have

$$\int_K vw \, \mathrm{d}x\mathrm{d}y = \int_K \lambda_1 \lambda_2 \, \mathrm{d}x\mathrm{d}y = \frac{1}{12}|K|.$$

On the other hand,

$$\int_{\triangle P_1 P_{12}^{\alpha} P_{12}^{\beta_1}} \lambda_2 \, \mathrm{d}x\mathrm{d}y = \frac{1}{6}\left(1 - \frac{1}{\sqrt{3}} + \beta_1\right) S_1,$$

$$\int_{\triangle P_1 P_{12}^{\beta_1} P_{13}^{\alpha}} \lambda_2 \, \mathrm{d}x\mathrm{d}y = \frac{1}{6}\beta_1 S_1,$$

$$(39) \qquad \int_{\triangle P_{31}^{\beta_2} P_{23}^{\beta_1} Q} \lambda_2 \, \mathrm{d}x\mathrm{d}y = \int_{\triangle P_{23}^{\beta_1} P_{12}^{\beta_2} Q} \lambda_2 \, \mathrm{d}x\mathrm{d}y = \frac{1}{3}\left(\frac{4}{3} - \beta_1 + \frac{\beta_2}{2}\right) S_2,$$

$$\int_{\triangle P_{12}^{\beta_1} P_{31}^{\beta_2} Q} \lambda_2 \, \mathrm{d}x\mathrm{d}y = \int_{\triangle P_{12}^{\beta_2} P_{31}^{\beta_1} Q} \lambda_2 \, \mathrm{d}x\mathrm{d}y = \frac{1}{3}\left(\frac{1}{3} + \frac{\beta_1}{2} + \frac{\beta_2}{2}\right) S_2,$$

$$\int_{\triangle P_{23}^{\beta_2} P_{12}^{\beta_1} Q} \lambda_2 \, \mathrm{d}x\mathrm{d}y = \int_{\triangle P_{31}^{\beta_1} P_{23}^{\beta_2} Q} \lambda_2 \, \mathrm{d}x\mathrm{d}y = \frac{1}{3}\left(\frac{4}{3} + \frac{\beta_1}{2} - \beta_2\right) S_2.$$

It follows from (39) that

$$\int_K \lambda_2 \lambda_1^* \, \mathrm{d}x\mathrm{d}y = \frac{5}{54}|K| + \frac{1}{12}\left(-4 - \frac{2}{\sqrt{3}} + 3\beta_1\right) S_1 + \frac{1}{18}\left(-1 - \frac{3}{2}\beta_1 + 3\beta_2\right) S_2.$$

Note that

$$S_1 = \frac{1}{4}\left(1 - \frac{1}{\sqrt{3}}\right)\beta_1|K|,$$

$$S_2 = \frac{1}{12}\left(2 - 3\beta_1\right)\left(3\beta_2 - 2\right)|K|.$$

Therefore, if β_1 and β_2 satisfy the relation (15), we deduce that

$$\int_K vw^* \, \mathrm{d}x\mathrm{d}y = \frac{1}{12}|K|.$$

In other words, (38) holds for $v = \lambda_2$ and $w = \lambda_1$. By the same arguments, we have

$$(40) \qquad \int_K \lambda_i \lambda_j \, \mathrm{d}x\mathrm{d}y = \int_K \lambda_i \lambda_j^* \, \mathrm{d}x\mathrm{d}y = \frac{1}{12}|K|, \quad i,j = 1,2,3 \text{ and } i \neq j.$$

It follows form (37) and (40) that

$$\int_K \lambda_1^2 \,\mathrm{d}x\mathrm{d}y = \int_K \lambda_1(1-\lambda_2-\lambda_3) \,\mathrm{d}x\mathrm{d}y = \int_K (\lambda_1^*-\lambda_2\lambda_1^*-\lambda_3\lambda_1^*) \,\mathrm{d}x\mathrm{d}y = \int_K \lambda_1\lambda_1^* \,\mathrm{d}x\mathrm{d}y,$$

where we have used the fact that $\lambda_1 + \lambda_2 + \lambda_3 = 1$ in the first and last equalities. Similarly, we get

$$\int_K \lambda_i^2 \,\mathrm{d}x\mathrm{d}y = \int_K \lambda_i\lambda_i^* \,\mathrm{d}x\mathrm{d}y, \quad i = 1,2,3.$$

Thus, (38) is verified and the proof is complete. $\qquad\square$

Remark 4.1. *From the process of proof in Lemma 4.1 and Lemma 4.2, we see that the Eqs. (36), (37) and (38) are valid independent the choice of ω, and moreover the Eqs. (36) and (37) are valid independent the choice of parameters β_1 and β_2.*

4.2. Application of the Aubin-Nitsche technique. We introduce an auxiliary problem: let $w \in H_0^1(\Omega)$ be the weak solution of

$$-\nabla \cdot (\Lambda\nabla w) = u - u_h \quad \text{in } \Omega,$$
$$w = 0 \qquad \text{on } \partial\Omega,$$

where u is the exact solution of (1) and (2), u_h is the bubble enriched quadratic finite volume element solution of (12). Then we have

(41) $$a(w,v) = (u - u_h, v), \quad \forall\, v \in H_0^1(\Omega),$$

where $a(\cdot,\cdot)$ is the finite element bilinear form defined by

(42) $$a(w,v) = \int_\Omega (\Lambda\nabla w) \cdot \nabla v \,\mathrm{d}x\mathrm{d}y.$$

Thus, by the regularity (c.f. [3, 13]), there exists a unique solution $w \in H_0^1(\Omega) \cap H^2(\Omega)$ such that

(43) $$\|w\|_2 \lesssim \|u - u_h\|_0.$$

Let $v = u - u_h$ in (41),

(44) $$\|u - u_h\|_0^2 = (u - u_h, u - u_h) = a(w - w_h, u - u_h) + a(w_h, u - u_h),$$

where $w_h = I_h w \in U_h^1$ is the piecewise linear interpolation such that for each vertex P_i, $i = 1,2,3$ of the triangular element K

$$w_h(P_i) = w(P_i).$$

By the standard approximation theory (c.f. [3, 13]), we obtain

(45) $$\|w - w_h\|_1 \lesssim h\|w\|_2.$$

It follows from the Cauchy-Schwarz inequality, (3), (45) and (35)

(46) $$|a(w - w_h, u - u_h)| \lesssim h^3\|w\|_2\|u\|_3.$$

For the second term $a(w_h, u-u_h)$ of (44), we note that u_h is the finite volume element solution of (12), then we do not have the Galerkin orthogonality. Fortunately, by the definition of u and u_h, we find that for the $w_h \in U_h^1 \subset U_h$,

$$a_h(u, w_h^*) = (f, w_h^*)$$

and

$$a_h(u_h, w_h^*) = (f, w_h^*).$$

It follows by subtraction that

(47) $$a_h(u - u_h, w_h^*) = 0.$$

Then by (47) and the equality $a(u, w_h) = (f, w_h)$, we get

$$(48) \quad a(w_h, u - u_h) = a(u - u_h, w_h) = a(u - u_h, w_h) - a_h(u - u_h, w_h^*) = E_1 + E_2,$$

where

$$E_1 = (f, w_h - w_h^*)$$

and

$$E_2 = a_h(u_h, w_h^*) - a(u_h, w_h).$$

We next estimate E_1 and E_2 respectively.

4.3. The estimate of $E_1 = (f, w_h - w_h^*)$.

Lemma 4.3. *Assume that $\mathcal{T}_h$ is shape regular and $f \in H^2(\Omega)$, α satisfies (14), $\beta_1 \in (0, 2/3)$ and $\beta_2 \in (2/3, 1)$ satisfy (15), then for all $w_h \in U_h^1$,*

$$(49) \qquad |(f, w_h - w_h^*)| \lesssim h^3 \|f\|_2 |w_h|_1,$$

where the hidden constant independent of the mesh size h.

Proof. Since $w_h \in U_h^1$, then by (38) and Cauchy-Schwarz inequality

$$|(f, w_h - w_h^*)| = |(f - I_h f, w_h - w_h^*)| \leq \|f - I_h f\|_0 \|w_h - w_h^*\|_0 \lesssim h^2 \|f\|_2 \|w_h - w_h^*\|_0.$$

For each $K \in \mathcal{T}_h$, suppose that

$$w_h = \sum_{i=1}^3 w_h(P_i) \lambda_i,$$

and denote

$$w_{21} = w_h(P_2) - w_h(P_1), \quad w_{31} = w_h(P_3) - w_h(P_1).$$

Then

$$w_h - w_h^* = w_{21}\lambda_2 + w_{31}\lambda_3, \text{ in polygon } \mathcal{V}_{K,P_1},$$

$$w_h - w_h^* = -\frac{1}{2}w_{21} + w_{21}\lambda_2 + w_{31}\lambda_3, \text{ in polygon } \mathcal{V}_{K,M_1},$$

$$w_h - w_h^* = -\frac{1}{3}(w_{21} + w_{31}) + w_{21}\lambda_2 + w_{31}\lambda_3, \text{ in polygon } \mathcal{V}_{K,Q}.$$

It follows that

$$\|w_h - w_h^*\|_{0, \mathcal{V}_{K,P_1}}^2 \leq \int_K (w_{21}\lambda_2 + w_{31}\lambda_3)^2 \, \mathrm{d}x\mathrm{d}y \lesssim h_K^2(w_{21}^2 + w_{31}^2),$$

and

$$\|w_h - w_h^*\|_{0, \mathcal{V}_{K,P_i}}^2 \lesssim h_K^2(w_{21}^2 + w_{31}^2), \quad i = 1, \cdots, 7.$$

Consequently,

$$\|w_h - w_h^*\|_{0,K}^2 \lesssim h_K^2(w_{21}^2 + w_{31}^2).$$

Note that $\mathcal{T}_h$ is shape regular, then by the scaling argument,

$$|w_h|_{1,K} \sim |w_h|_{1,\widehat{K}}.$$

On the other hand, by a direct calculation,

$$|w_h|_{1,\widehat{K}}^2 = \frac{1}{2}\left(w_{21}^2 + w_{31}^2\right).$$

Therefore, we obtain

$$(50) \qquad \|w_h - w_h^*\|_{0,K} \lesssim h_K |w_h|_{1,K}$$

and

$$\|w_h - w_h^*\|_0^2 = \sum_{K \in \mathcal{T}_h} \|w_h - w_h^*\|_{0,K}^2 \lesssim \sum_{K \in \mathcal{T}_h} h_K^2 |w_h|_{1,K}^2 \lesssim h^2 |w_h|_1^2,$$

and the desired result (49) is proved. $\qquad\qquad\qquad\qquad\qquad\qquad\qquad\square$

4.4. The estimate of $E_2 = a_h(u_h, w_h^*) - a(u_h, w_h)$.

Lemma 4.4. *Assume that $\mathcal{T}_h$ is shape regular, $\Lambda \in W^{3,\infty}(\Omega)$, $u \in H^3(\Omega)$. Then, under the assumption* (**A1**), *for all $w_h \in U_h^1$, we have*

$$(51) \qquad\qquad |a_h(u_h, w_h^*) - a(u_h, w_h)| \lesssim h^3 \|u\|_3 |w_h|_1.$$

Proof. Firstly, let us discuss the relationship between the finite volume element bilinear form $a_h(u_h, w_h^*)$ and finite element bilinear form $a(u_h, w_h)$. Note that $w_h^*(P) = 0$, $\forall P \in \mathcal{N}_h \cap \partial\Omega$, then it follows from (13) and the Green's formula that

$$a_h(u_h, w_h^*) = -\sum_{K \in \mathcal{T}_h} \sum_{P \in \mathcal{N}_h} \int_{\partial \mathcal{V}_P \cap K} (\Lambda \nabla u_h) \cdot \boldsymbol{n} w_h^* \, \mathrm{d}s$$

$$= \sum_{K \in \mathcal{T}_h} \int_{\partial K} (\Lambda \nabla u_h) \cdot \boldsymbol{n} w_h^* \, \mathrm{d}s - \sum_{K \in \mathcal{T}_h} \int_K \nabla \cdot (\Lambda \nabla u_h) w_h^* \, \mathrm{d}x\mathrm{d}y,$$

and from (42)

$$a(u_h, w_h) = \sum_{K \in \mathcal{T}_h} \int_{\partial K} (\Lambda \nabla u_h) \cdot \boldsymbol{n} w_h \, \mathrm{d}s - \sum_{K \in \mathcal{T}_h} \int_K \nabla \cdot (\Lambda \nabla u_h) w_h \, \mathrm{d}x\mathrm{d}y.$$

Combining the above two equalities,

$$E_2 = a_h(u_h, w_h^*) - a(u_h, w_h) = E_{21} + E_{22},$$

where

$$E_{21} = \sum_{K \in \mathcal{T}_h} \int_K \nabla \cdot (\Lambda \nabla u_h)(w_h - w_h^*) \, \mathrm{d}x\mathrm{d}y$$

and

$$E_{22} = \sum_{K \in \mathcal{T}_h} \int_{\partial K} (\Lambda \nabla u_h) \cdot \boldsymbol{n}(w_h^* - w_h) \, \mathrm{d}s.$$

Next, we estimate E_{21} and E_{22} respectively. For E_{21}, by (38) and (50), we deduce that

$$|E_{21}| = \left| \sum_{K \in \mathcal{T}_h} \int_K (\nabla \cdot (\Lambda \nabla u_h) - I_h(\nabla \cdot (\Lambda \nabla u_h)))(w_h - w_h^*) \, \mathrm{d}x\mathrm{d}y \right|$$

$$\leq \sum_{K \in \mathcal{T}_h} \|\nabla \cdot (\Lambda \nabla u_h) - I_h(\nabla \cdot (\Lambda \nabla u_h))\|_{0,K} \|w_h - w_h^*\|_{0,K}$$

$$\lesssim \sum_{K \in \mathcal{T}_h} h_K^3 |\nabla \cdot (\Lambda \nabla u_h)|_{2,K} |w_h|_{1,K}$$

$$\lesssim \sum_{K \in \mathcal{T}_h} h_K^3 \|u_h\|_{3,K} |w_h|_{1,K},$$

where in the last inequality we have used the facts that $\Lambda \in W^{3,\infty}(\Omega)$ and $|u_h|_{4,K} = 0$. On the other hand, by the triangle inequality and inverse inequality

$$\|u_h\|_{3,K} \leq \|u_h - u_I\|_{3,K} + \|u_I\|_{3,K}$$

$$\lesssim h_K^{-2} \|u_h - u_I\|_{1,K} + \|u - u_I\|_{3,K} + \|u\|_{3,K}$$

$$\lesssim h_K^{-2} \|u - u_h\|_{1,K} + \|u\|_{3,K}.$$

Consequently, we get

$$|E_{21}| \lesssim \sum_{K \in \mathcal{T}_h} \left(h_K \|u - u_h\|_{1,K} + h_K^3 \|u\|_{3,K} \right) |w_h|_{1,K}$$

$$\lesssim h \|u - u_h\|_1 |w_h|_1 + h^3 \|u\|_3 |w_h|_1$$

$$\lesssim h^3 \|u\|_3 |w_h|_1,$$

where we have used the fact (35) in the last inequality.

To estimate E_{22}, let Λ_M be the piecewise constant interpolation on each edge of triangular element K, satisfying

$$\Lambda_M(x, y) = \Lambda(M_i), \quad \forall (x, y) \in P_i P_{i+1}, \ i = 1, 2, 3.$$

Note that $(\Lambda_M \nabla u_h) \cdot \boldsymbol{n}$ is a quadratic polynomial on ∂K and ∇u is continuous across ∂K, then by (36) and $w_h^*|_{\partial \Omega} = w_h|_{\partial \Omega} = 0$, we have

$$\sum_{K \in \mathcal{T}_h} \int_{\partial K} (\Lambda_M \nabla u_h) \cdot \boldsymbol{n} (w_h^* - w_h) \, \mathrm{d}s = 0$$

and

$$\sum_{K \in \mathcal{T}_h} \int_{\partial K} ((\Lambda - \Lambda_M) \nabla u) \cdot \boldsymbol{n} (w_h^* - w_h) \, \mathrm{d}s = 0.$$

Using the fact $\Lambda \in W^{3,\infty}(\Omega)$, we obtain

$$|E_{22}| = \left| \sum_{K \in \mathcal{T}_h} \int_{\partial K} ((\Lambda - \Lambda_M) \nabla (u_h - u)) \cdot \boldsymbol{n} (w_h^* - w_h) \, \mathrm{d}s \right|$$

$$\leq \sum_{K \in \mathcal{T}_h} \int_{\partial K} |(\Lambda - \Lambda_M) \nabla (u_h - u)| |w_h^* - w_h| \, \mathrm{d}s$$

$$\lesssim \sum_{K \in \mathcal{T}_h} h_K \|\nabla (u - u_h)\|_{0,\partial K} \|w_h - w_h^*\|_{0,\partial K}$$

$$\lesssim \left(\sum_{K \in \mathcal{T}_h} h_K \|\nabla (u - u_h)\|_{0,\partial K}^2 \right)^{\frac{1}{2}} \left(\sum_{K \in \mathcal{T}_h} h_K \|w_h - w_h^*\|_{0,\partial K}^2 \right)^{\frac{1}{2}}.$$

By the trace theorem (c.f. [3]), we get

$$\left(\sum_{K \in \mathcal{T}_h} h_K \|\nabla (u - u_h)\|_{0,\partial K}^2 \right)^{\frac{1}{2}} \lesssim \left(\sum_{K \in \mathcal{T}_h} \left(|u - u_h|_{1,K}^2 + h_K^2 |u - u_h|_{2,K}^2 \right) \right)^{\frac{1}{2}}$$

$$\lesssim h^2 \|u\|_3$$

and

$$\left(\sum_{K \in \mathcal{T}_h} h_K \|w_h - w_h^*\|_{0,\partial K}^2 \right)^{\frac{1}{2}} \lesssim \left(\sum_{K \in \mathcal{T}_h} \left(\|w_h - w_h^*\|_{0,K}^2 + h_K^2 |w_h|_{1,K}^2 \right) \right)^{\frac{1}{2}}$$

$$\lesssim h |w_h|_1,$$

where we have used the fact that

$$|u - u_h|_{2,K} \leq |u - u_I|_{2,K} + |u_I - u_h|_{2,K}$$

$$\lesssim h_K \|u\|_{3,K} + h_K^{-1} \|u_I - u_h\|_{1,K}$$

$$\lesssim h_K \|u\|_{3,K} + h_K^{-1} \|u - u_h\|_{1,K}.$$

Consequently,

$$|E_{22}| \lesssim h^3 \|u\|_3 |w_h|_1.$$

Therefore, we have

$$|E_2| = |a_h(u_h, w_h^*) - a(u_h, w_h)| \leq |E_{21}| + |E_{22}| \lesssim h^3 \|u\|_3 |w_h|_1$$

and (51) is proved.   □

Remark 4.2. *From the process of proof in Lemma 4.4, we see that if the coefficient Λ is piecewise constant with respect to $\mathcal{T}_h$, then $E_{21} = E_{22} = 0$, thus $E_2 = 0$.*

4.5. Convergence rate of L^2 error estimates.

Theorem 4.1. *Let u be the exact solution of* (1) *and* (2), *u_h be the finite volume element solution of* (12). *Assume that $\mathcal{T}_h$ is shape regular, $\Lambda \in W^{3,\infty}(\Omega)$, $u \in H^3(\Omega)$, $f \in H^2(\Omega)$. Then, under the assumption (**A1**), we have*

$$(52) \qquad\qquad \|u - u_h\|_0 \lesssim h^3(\|u\|_3 + \|f\|_2).$$

Proof. Combining (44), (46), (48), (49), (51) and the fact

$$|w_h|_1 \leq |w - w_h|_1 + |w|_1 \lesssim \|w\|_2$$

yield that

$$\|u - u_h\|_0^2 \lesssim h^3(\|u\|_3 + \|f\|_2)\|w\|_2 \lesssim h^3(\|u\|_3 + \|f\|_2)\|u - u_h\|_0,$$

where we have used (43) in the last inequality. The proof is complete.   □

Remark 4.3. *From the process of proof in Theorem 4.1, we see that once the H^1 error estimate* (35) *is obtained, the L^2 error estimate* (52) *is valid independent the choice of ω. However, ω is crucial in the coercivity analysis, e.g., [45, 46, 48].*

Remark 4.4. *If α satisfies* (14), *then the orthogonal condition* (36) *holds. If $\beta_1 \in (0, 2/3)$ and $\beta_2 \in (2/3, 1)$ satisfy* (15), *then the orthogonal condition* (38) *holds. The two orthogonal conditions play an important role in our L^2 error estimates.*

5. Numerical examples

In this section, we present several numerical examples to validate the theoretical findings of this paper. The numerical experiments are implemented on a personal computer with 2.16 GHz CPU and 4 Gb RAM and Matlab R2016a is used as the testing platform.

Examples 5.1, 5.2 and 5.3 are designed for constant, variable and discontinuous coefficients, respectively, while Example 5.4 is a highly anisotropic diffusion problem. In these examples, we choose $\Omega = [0,1]^2$ and employ four types of triangular meshes. The first kind of mesh (Mesh I) is a uniform triangular one, see Figure 8(a), and the coordinates of the vertices are given by

$$x_{ij} = (i-1)h, \ y_{ij} = (j-1)h, \quad 1 \leq i, \ j \leq n+1,$$

where $h = 1/n$ is the mesh size. The third mesh (Mesh III) is a random triangular one, see Figure 8(c), which is obtained by randomly disturbing the interior vertices of Mesh I and keeping the connections unchanged. Specifically, the coordinates of the interior vertices in Mesh III are

$$x_{ij} := x_{ij} + \omega r_x h, \ y_{ij} := y_{ij} + \omega r_y h, \quad 2 \leq i, \ j \leq n,$$

where $\omega \in [0, 0.5]$ is the disturbance coefficient, while r_x and r_y are two random numbers that belong to $(-1, 1)$. The second mesh (Mesh II) is also a random one where the interior vertices are only allowed to be disturbed along y direction, see

(a) Mesh I   (b) Mesh II   (c) Mesh III
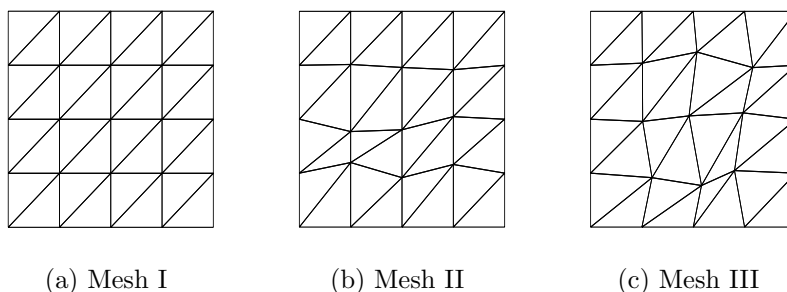
FIGURE 8. Three mesh types used in the numerical examples.

(a) first level   (b) second level   (c) third level
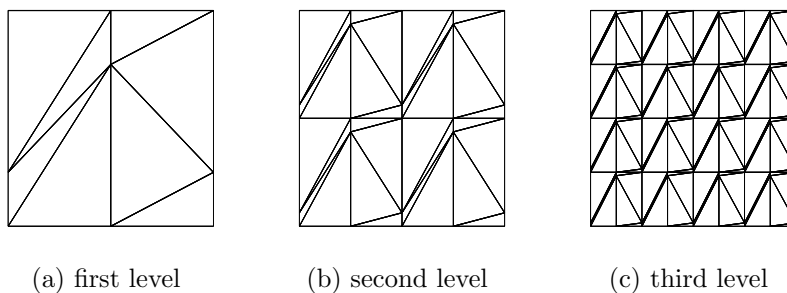
FIGURE 9. Mesh IV.

Figure 8(b). The last mesh (Mesh IV, see Figure 9) is constructed by the uniform mesh such that when j is an even number,

$$y_{ij} := y_{i,j-1} + h^2, \quad i = 1, 3, \cdots, n+1,$$
$$y_{ij} := y_{i,j+1} - h^2, \quad i = 2, 4, \cdots, n.$$

In these examples, we choose $\omega = 0.25$ for Mesh II and Mesh III. Let

(53) $$\theta_{\min} = \min_{K \in \mathcal{T}_h} \theta_K,$$

where θ_K is the minimum interior angle of K. The $\theta_{\min}$ of these meshes are presented in Table 1, one can see that for the Mesh IV, $\theta_{\min} \to 0°$ provided $h \to 0$. Here we investigate the numerical performance of the following seven finite volume element schemes:

- Bubble 1/4: $\alpha = (3 - \sqrt{3})/6$, $\beta_1 = 1/4$, $\beta_2 = (135 + \sqrt{5265 - 2400\sqrt{3}})/240$. This is the scheme presented in this paper.
- Bubble 1/3: $\alpha = (3 - \sqrt{3})/6$, $\beta_1 = 1/3$, $\beta_2 = (7 + \sqrt{25 - 8\sqrt{3}})/12$. This is the scheme presented in this paper.
- TianChen91: $\alpha = 1/3$, $\beta_1 = 1/3$, $\beta_2 = 2/3$. This scheme was presented in [33] by Tian and Chen in 1991.
- Emonot92: $\alpha = 1/6$, $\beta_1 = 1/4$, $\beta_2 = 2/3$. This scheme was presented in [15] by Emonot in 1992.
- Liebau96: $\alpha = 1/4$, $\beta_1 = 1/3$, $\beta_2 = 2/3$. This scheme was presented in [24] by Liebau in 1996.
- WangLi16: $\alpha = (3 - \sqrt{3})/6$, $\beta_1 = (6 + \sqrt{3} - \sqrt{21 + 6\sqrt{3}})/9$, $\beta_2 = 2/3$. This scheme was presented in [36] by Wang and Li in 2016.

TABLE 1. The minimum angle $\theta_{\min}$ for the four types of triangular meshes.

h	Mesh I	Mesh II	Mesh III	Mesh IV
1/2	45.00°	33.89°	32.90°	11.31°
1/4	45.00°	26.51°	22.19°	3.95°
1/8	45.00°	24.25°	17.42°	1.67°
1/16	45.00°	22.42°	12.94°	0.77°
1/32	45.00°	21.02°	9.91°	0.37°
1/64	45.00°	20.54°	12.01°	0.18°

- Zou17: $\alpha = (3 - \sqrt{3})/6$, $\beta_1 = (1 - 1/\sqrt{3})/2$, $\beta_2 = 2/3$. This scheme was presented in [48] by Zou in 2017.

Example 5.1. We consider the problem (1) and (2), choose the constant diffusion coefficient and right hand side function

$$\Lambda(x,y) = \begin{pmatrix} 1 & 1 \\ 1 & 2 \end{pmatrix}, \quad f(x,y) = 3\pi^2 \sin(\pi x) \sin(\pi y) - 2\pi^2 \cos(\pi x) \cos(\pi y),$$

which allows the exact solution

$$u(x,y) = \sin(\pi x) \sin(\pi y).$$

The numerical results of the seven schemes on Mesh I are graphically depicted in Figure 10 as log-log plots of the discrete errors versus the characteristic mesh size h. One can observe that for the three schemes: Bubble 1/4, Bubble 1/3 and WangLi16, the convergence order in H^1 and L^2 error norm are all of 2 and 3 respectively, which validate the theoretical results in Theorem 3.2 and Theorem 4.1. For the four schemes: TianChen91, Emonot92, Liebau96 and Zou17, we can see that the convergence order in H^1 error norm are all of 2. However, the errors in L^2 norm are all approximately one order lower than the optimal order 3 even though Mesh I is uniform.

The relation between the error orders and bubble enriched schemes (15) is depicted in Figure 11, where the convergence orders are computed from the errors on the finest two levels of Mesh I. From Figure 11, one can see that the convergence order in H^1 and L^2 error norm are all of 2 and 3 respectively provided α satisfies (14), $\beta_1 \in (0, 2/3)$ and $\beta_2 \in (2/3, 1)$ satisfy (15), namely the theoretical results in Theorem 3.2 and Theorem 4.1 are verified again.

The numerical errors on Mesh II, III and IV are graphically depicted in Figures 12, 13 and 14 respectively. One can observe that the numerical results are similar to Mesh I. Moreover, we observe that the existence and uniqueness of the finite volume element solution and corresponding convergence order are all independent of the minimal angle $\theta_{\min}$ of the meshes, even though $\theta_{\min} \to 0°$ for the Mesh IV.

Example 5.2. We solve the problem (1) and (2), where the variable diffusion coefficient and right hand side function are given by

$$\Lambda(x,y) = \begin{pmatrix} 1 + x & \frac{1}{2}(x - y) \\ \frac{1}{2}(x - y) & 1 + y \end{pmatrix}, \quad f(x,y) = -2(2 + x)e^{x+y}.$$

This problem has the analytic solution

$$u(x,y) = e^{x+y}.$$

The numerical errors on Mesh IV are similar to Example 5.1, see Figure 15. For these schemes, the H^1 errors are of order 2, while the L^2 error order are 3 for the

(a) H^1 errors   (b) L^2 errors
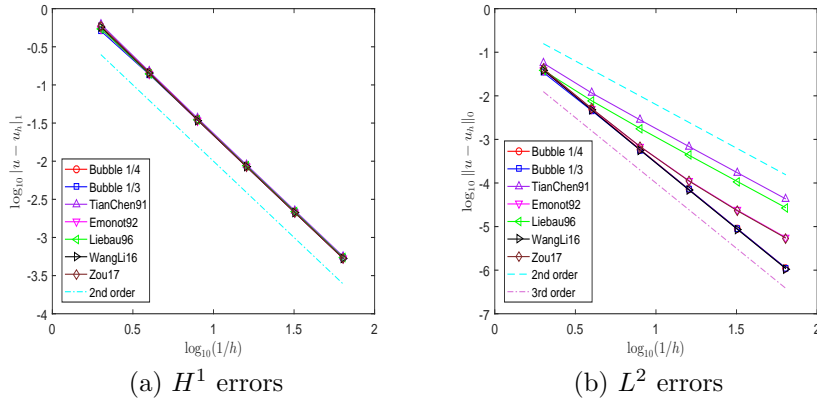
FIGURE 10. Numerical errors for Example 5.1 on Mesh I.
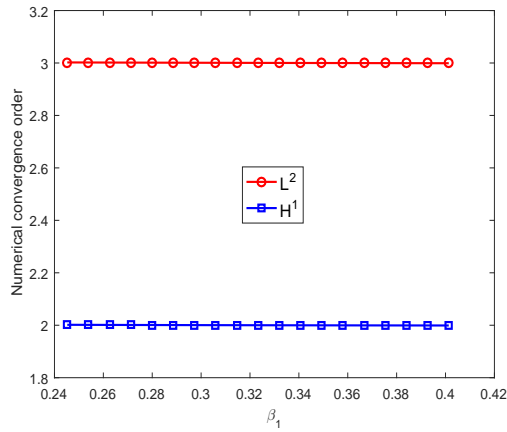
FIGURE 11. Numerical convergence order of the class of bubble enriched schemes (15) for Example 5.1 on Mesh I.

(a) H^1 errors   (b) L^2 errors
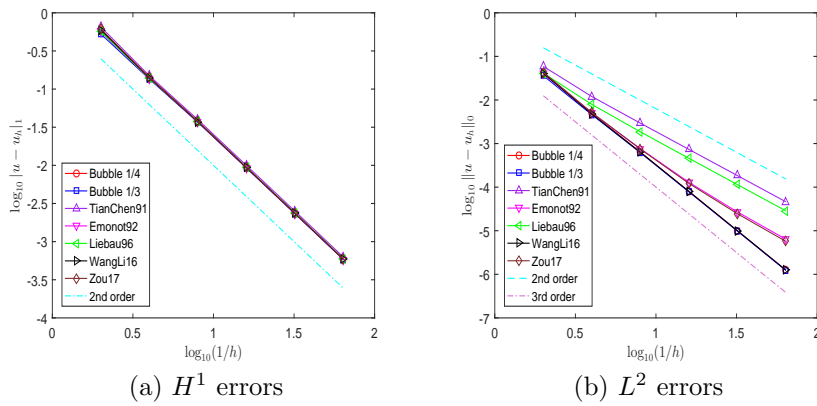
FIGURE 12. Numerical errors for Example 5.1 on Mesh II.

(a) H^1 errors

(b) L^2 errors
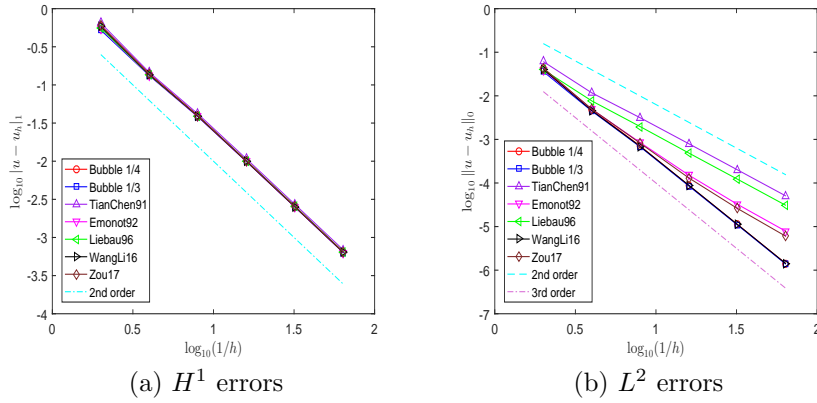
FIGURE 13. Numerical errors for Example 5.1 on Mesh III.

(a) H^1 errors

(b) L^2 errors
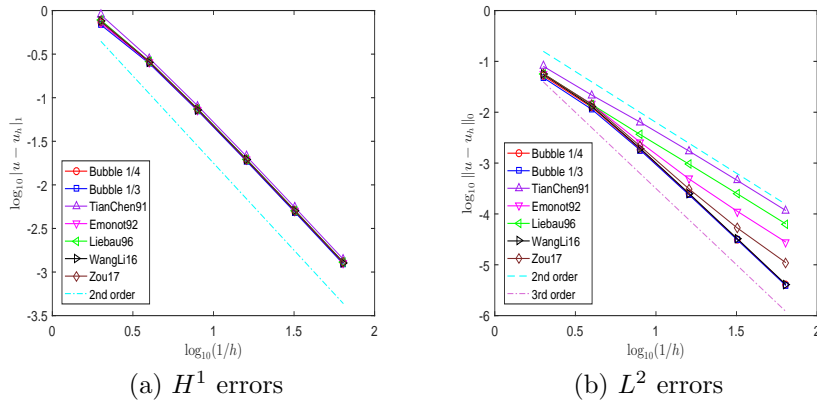
FIGURE 14. Numerical errors for Example 5.1 on Mesh IV.

(a) H^1 errors

(b) L^2 errors
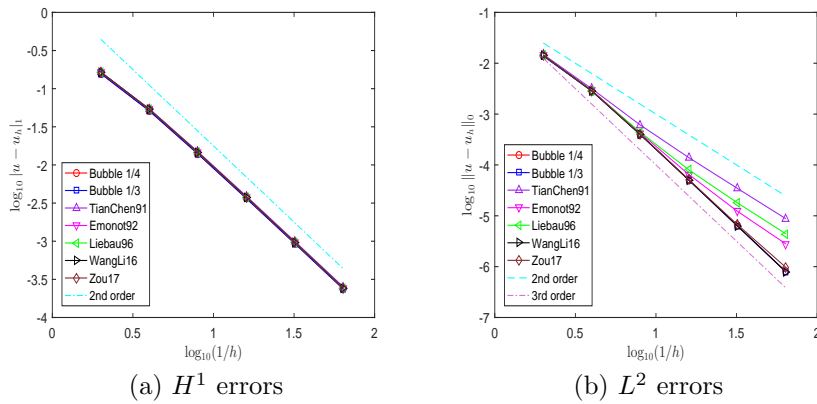
FIGURE 15. Numerical errors for Example 5.2 on Mesh IV.

three schemes Bubble 1/4, Bubble 1/3 and WangLi16, and approximately 2 for the rest four schemes. For the other three meshes, there also have similar results.

(a) H^1 errors   (b) L^2 errors
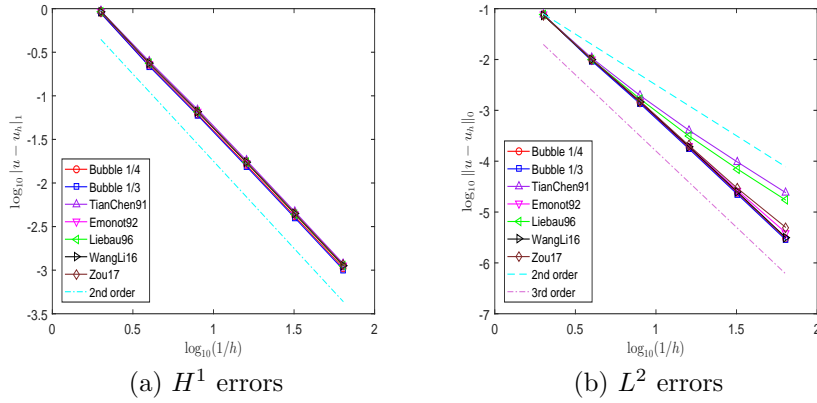
FIGURE 16. Numerical errors for Example 5.3 on Mesh IV.

Example 5.3. We still solve the problem (1) and (2), where the discontinuous anisotropic diffusion coefficient is

$$\Lambda(x,y) = \begin{cases} \begin{pmatrix} 1 & 0 \\ 0 & 1 \end{pmatrix}, & x \leq 0.5, \\[2em] \begin{pmatrix} 1 & 1.5 \\ 1.5 & 3 \end{pmatrix}, & x > 0.5. \end{cases}$$

The exact solution and corresponding right hand side function are given by

$$u(x,y) = \begin{cases} 4xe^{x+y}, & x \leq 0.5, \\ (x+1.5)e^{x+y}, & x > 0.5, \end{cases} \qquad f(x,y) = \begin{cases} -8(x+1)e^{x+y}, & x \leq 0.5, \\ -(7x+15.5)e^{x+y}, & x > 0.5. \end{cases}$$

Since in this example the diffusion tensor is discontinuous across the line $x = 0.5$, then we use the Mesh I, Mesh II and Mesh IV. On Mesh IV, the numerical errors are presented in Figure 16, where we see that the convergence orders of H^1 and L^2 errors of the seven schemes are similar to the previous examples. For the Mesh I and Mesh II, there also have similar results.

Example 5.4. We solve a highly anisotropic diffusion problem which was presented in [5], where

$$\Lambda(x,y) = \begin{pmatrix} \cos\theta & \sin\theta \\ -\sin\theta & \cos\theta \end{pmatrix} \begin{pmatrix} 1 & 0 \\ 0 & \kappa \end{pmatrix} \begin{pmatrix} \cos\theta & -\sin\theta \\ \sin\theta & \cos\theta \end{pmatrix}$$

and

$$u(x,y) = \frac{\arctan\left(0.5 - (x-0.5)^2 - (y-0.5)^2\right)}{\arctan 0.5}.$$

(a) H^1 errors   (b) L^2 errors
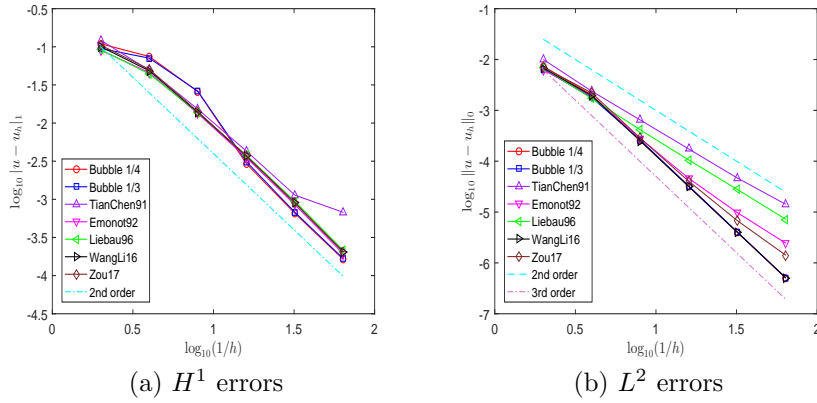
FIGURE 17. Numerical errors for Example 5.4 on Mesh IV.

TABLE 2. The running time (minute) of numerical errors for Example 5.4 on Mesh IV.

Bubble 1/4	Bubble 1/3	TianChen91	Emonot92	Liebau96	WangLi16	Zou17
4.71 m	4.69 m	2.99 m	3.06 m	3.05 m	3.01 m	3.17 m

The right hand side function is given by

$$
f(x, y) = \frac{2}{\left(1 + (x + y - x^2 - y^2)^2\right)^2 \arctan 0.5} \Bigg((\kappa + 1)\left(1 + (x + y - x^2 - y^2)^2\right)
$$
$$
+ 8(\kappa - 1)(x - 0.5)(y - 0.5)\left(x + y - x^2 - y^2\right)\sin\theta\cos\theta
$$
$$
+ 4\left(x + y - x^2 - y^2\right)\Big((x - 0.5)^2\left(\kappa \sin^2\theta + \cos^2\theta\right)
$$
$$
+ (y - 0.5)^2\left(\sin^2\theta + \kappa\cos^2\theta\right)\Big)\Bigg).
$$

In this example, we choose

$$
\kappa = 10^4, \quad \theta = \frac{\pi}{6}.
$$

The numerical errors on Mesh IV are similar to the previous examples, see Figure 17. For the other three meshes, there also have similar results. On Mesh IV, the running time (minute) of these schemes are presented in Table 2. We observe that the running time of bubble enriched quadratic schemes are greater than the classic quadratic schemes, since the new schemes have one more degree of freedom on each triangular element. Note that the exact solution $u(x, y) \geq 0$, $\forall (x, y) \in \Omega$, here we test the positivity preserving property of these schemes. The results are given in Table 3, where

$$
u_{\min} = \min_{P \in \mathcal{N}_h^\circ} u_h(P),
$$

and $\mathcal{N}_h^\circ$ includes the barycenters, we observe that these schemes all produce non-negative solutions at each $P \in \mathcal{N}_h^\circ$.

6. Conclusions

This paper presents a class of bubble enriched quadratic FVE schemes over triangular meshes for solving anisotropic diffusion problems. The trial function

TABLE 3. The values of $u_{\min}$ for Example 5.4 on Mesh IV.

h	1/2	1/4	1/8	1/16	1/32	1/64
Bubble 1/4	0.456073	0.207996	0.097254	0.046800	0.022935	0.011350
Bubble 1/3	0.455906	0.207945	0.097252	0.046800	0.022935	0.011350
TianChen91	0.454781	0.208081	0.097266	0.046801	0.022935	0.011350
Emonot92	0.455069	0.207958	0.097253	0.046800	0.022935	0.011350
Liebau96	0.454921	0.208006	0.097258	0.046801	0.022935	0.011350
WangLi16	0.454967	0.207982	0.097256	0.046801	0.022935	0.011350
Zou17	0.454968	0.207981	0.097256	0.046801	0.022935	0.011350

space consists of a quadratic finite element and an element-wise bubble functions. Under the assumption (**A1**), we proved that $|u - u_h|_1 = \mathcal{O}(h^2)$ and $\|u - u_h\|_0 = \mathcal{O}(h^3)$. We mention that the assumption (**A1**) is derived from element analysis approach and it is just a sufficient condition to ensure (21). Moreover, from Figures 6 and 7, we see that the assumption (**A1**) is valid under a certain minimum angle condition. On the other hand, for the Mesh IV used in Section 5, we have $\theta_{\min} \to 0°$ (the $\theta_{\min}$ defined by (53)) provided $h \to 0$, and the numerical results indicate that there exists one unique FVE solution even though $\theta_{\min}$ is very small. Therefore, more studies about the coercivity analysis should be developed further, and we expect that all the FVE schemes are unconditionally stable.

Acknowledgments

References

[1] Bank, R. E., Rose, D. J.: Some error estimates for the box method. SIAM J. Numer. Anal., 24, 777-787 (1987).

[2] Barth, T., Ohlberger, M.: Finite Volume Methods: Foundation and Analysis. In: Encyclopedia of Computational Mechanics, vol. 1, chapter 15. Wiley (2004).

[3] Braess, D.: Finite Elements: Theory, Fast Solvers, and Applications in Solid Mechanics, 3rd ed. Cambridge University Press (2007).

[4] Cai, Z.: On the finite volume element method. Numer. Math., 58, 713-735 (1991).

[5] Camier, J., Hermeline, F.: A monotone nonlinear finite volume method for approximating diffusion operators on general meshes. Int. J. Numer. Meth. Engng., 107, 496-519 (2016).

[6] Chen, L.: A new class of high order finite volume methods for second order elliptic equations. SIAM J. Numer. Anal., 47, 4021-4043 (2010).

[7] Chen, Y., Li, Y.: Optimal bicubic finite volume methods on quadrilateral meshes. Adv. Appl. Math. Mech., 7, 454-471 (2015).

[8] Chen, Z.: A generalized difference method for the equations of heat conduction. Acta Sci. Natur. Univ. Sunyatseni, 29, 6-13 (1990).

[9] Chen, Z.: L^2 error estimates for generalized difference method. Acta Sci. Natur. Univ. Sunyatseni, 33, 22-28 (1994).

[10] Chen, Z., Li, R., Zhou, A.: A note on the optimal L^2-estimate of the finite volume element method. Adv. Comput. Math., 16, 291-303 (2002).

[11] Chen, Z., Wu, J., Xu, Y.: Higher-order finite volume methods for elliptic boundary value problems. Adv. Comput. Math., 37, 191-253 (2012).

[12] Chen, Z., Xu, Y., Zhang, Y.: A construction of higher-order finite volume methods. Math. Comp., 84, 599-628 (2015).

[13] Ciarlet, P.:   The finite element method for elliptic problems. North-Holland, Amsterdam (1978).

[14] Du, Y., Li, Y., Sheng, Z.:   Quadratic finite volume method for a nonlinear elliptic problem. Adv. Appl. Math. Mech., 11, 838-869 (2019).

[15] Emonot, Ph.:   Methodes de volumes elements finis: applications aux equations de Navier-Stokes et resultats de convergence. Dissertation, Lyon (1992).

[16] Ewing, R. E., Lin, T., Lin, Y.:   On the accuracy of the finite volume element method based on piecewise linear polynomials. SIAM J. Numer. Anal., 39, 1865-1888 (2002).

[17] Hackbusch, W.:   On first and second order box schemes. Computing, 41, 277-296 (1989).

[18] Hong, Q., Wu, J.:   Coercivity results of a modified Q_1-finite volume element scheme for anisotropic diffusion problems. Adv. Comput. Math., 44, 897-922 (2018).

[19] Huang, J., Xi, S.:   On the finite volume element method for general self-adjoint elliptic problems. SIAM J. Numer. Anal., 35, 1762-1774 (1998).

[20] Jin, G., Li, H., Zhang, Q., Zou, Q.:   Linear and quadratic finite volume methods on triangular meshes for elliptic equations with singular solutions. Int. J. Numer. Anal. Mod., 13, 244-264 (2016).

[21] LeVeque, R. J.:   Finite Volume Methods for Hyperbolic Problems. Cambridge Texts in Applied Mathematics. Cambridge University Press, Cambridge (2002).

[22] Li, R., Chen, Z., Wu, W.:   The generalized difference methods for partial differential equations: Numerical analysis of finite volume methods. Marcel Dikker, New York (2000).

[23] Li, Y., Li, R.:   Generalized difference methods on arbitrary quadrilateral networks. J. Comput. Math., 17, 653-672 (1999).

[24] Liebau, F.:   The finite volume element method with quadratic basis functions. Computing, 57, 281-299 (1996).

[25] Lin, Y., Liu, J., Yang, M.:   Finite volume element methods: an overview on recent developments. Int. J. Numer. Anal. Mod., 4, 14-34 (2013).

[26] Lin, Y., Yang, M., Zou, Q.: L^2 error estimates for a class of any order finite volume schemes over quadrilateral meshes. SIAM J. Numer. Anal., 53, 2030-2050 (2015).

[27] Lv, J., Li, Y.: L^2 error estimate of the finite volume element methods on quadrilateral meshes. Adv. Comput. Math., 33, 129-148 (2010).

[28] Lv, J., Li, Y.: L^2 error estimates and superconvergence of the finite volume element methods on quadrilateral meshes. Adv. Comput. Math., 37, 393-416 (2012).

[29] Lv, J., Li, Y.:   Optimal biquadratic finite volume element methods on quadrilateral meshes. SIAM J. Numer. Anal., 50, 2379-2399 (2012).

[30] Moukalled, F., Mangani, L., Darwish, M.:   The Finite Volume Method in Computational Fluid Dynamics: An Advanced Introduction with OpenFoam and Matlab, Springer, Switherland (2016).

[31] Petrila, T., Trif, D.:   Basics of Fluid Mechanics and Introduction to Computational Fluid Dynamics. Springer (2005).

[32] Schmidt, T.:   Box schemes on quadrilateral meshes. Computing, 51, 271-292 (1993).

[33] Tian, M., Chen, Z.:   Quadratic element generalized differential methods for elliptic equations. Numer. Math. J. Chin. Univ., 13, 99-113 (1991).

[34] Versteeg, H. K., Malalasekra, W.:   An Introduction to Computational Fluid Dynamics: the Finite Volume Method, 2nd ed. Pearson Education, England (2007).

[35] Wang, P., Zhang, Z.:   Quadratic finite volume element method for the air pollution model. Int. J. Comput. Math., 87, 2925-2944 (2010).

[36] Wang, X., Li, Y.: L^2 error estimates for high order finite volume methods on triangular meshes. SIAM J. Numer. Anal., 54, 2729-2749 (2016).

[37] Xiong, Z., Deng, K.:   A quadratic triangular finite volume element method for a semilinear elliptic equation. Adv. Appl. Math. Mech., 9, 186-204 (2017).

[38] Xu, J., Zou, Q.:   Analysis of linear and quadratic simplicial finite volume methods for elliptic equations. Numer. Math., 111, 469-492 (2009).

[39] Yang, M.:   Quadratic finite volume element methods for nonlinear parabolic equations. Numer. Math. J. Chin. Univ., 26, 257-266 (2004).

[40] Yang, M.:   Error estimates of quadratic finite volume element methods for nonlinear parabolic systems. Acta Math., Appl., Sin., 29, 29-38 (2006).

[41] Yang, M.:   A second-order finite volume element method on quadrilateral meshes for elliptic equations. ESAIM: M2AN, 40, 1053-1067 (2006).

[42] Yang, M., Liu, J., Lin, Y.:   Quadratic finite-volume methods for elliptic and parabolic problems on quadrilateral meshes: optimal-order errors based on Barlow points. IMA J. Numer. Anal., 33, 1342-1364 (2013).

[43] Zhang, Z., Zou, Q.: Some recent advances on vertex centered finite volume element methods for elliptic equations. Sci. China Math., 56, 2507-2522 (2013).

[44] Zhang, Z., Zou, Q.:   Vertex-centered finite volume schemes of any order over quadrilateral meshes for elliptic boundary value problems. Numer. Math., 130, 363-393 (2015).

[45] Zhou, Y., Wu, J.:   A family of quadratic finite volume element schemes over triangular meshes for elliptic equations. Comput. Math. Appl., 79, 2473-2491 (2020).

[46] Zhou, Y., Wu, J.:   A unified analysis of a class of quadratic finite volume element schemes on triangular meshes. Adv. Comput. Math., 46, 71 (2020).

[47] Zhu, P., Li, R.:   Generalized difference methods for second order elliptic partial differential equations. II. Quadrilateral subdivision. Numer. Math. J. Chin. Univ., 4, 360-375 (1982).

[48] Zou, Q.:   An unconditionally stable quadratic finite volume scheme over triangular meshes for elliptic equations. J. Sci. Comput., 70, 112-124 (2017).

School of Data and Computer Science, Sun Yat-Sen University, Guangzhou, 510275, China
E-mail: zhouyh9@mail2.sysu.edu.cn